CO1-1 Morphological Control in PS-b-PI-b-PDMS Triblock Copolymer by Mixed-Solvent

M.Takenaka, YiChin Wang, H. Ogawa

Institute for Chemical Research, Kyoto University

Introduction

Various kinds of periodic morphologies in blockcopolymers have been extensively studied over decades. In addition, several researches have put emphasis to- ward complex systems, such as multiblock copolymers and non-linear block copolymers, and broaden the ex- tent that various microdomain morphologies and different microdomain sizes can be accessed. In equilibrium state of strong segregation limit, the morpholo- gies of block copolymers depend on only volume fraction of each constituent polymer and their architec- tures, and the synthesis process are very important too control their morphologies. In this study, we will demonstrate the tunability of the microdomain mor- phology in polystyrene-*block*-polyisoprene-*block*-polydimethylsiloxane (SID) triblock copolymer produced from its solution of mixed solvent of toluene and n-decane. By varying the weight ratio and the concentration of the mixed solvent, corresponding ordered microdomain morphologies such as spheres, hexagonally-packed cylinders, lamellae and OTDD network structure could be easily formed in the polymer solu- tion. Moreover, these ordered microdomain morpholo- gies found in the solution can be preserved in thin bulk state.

Experimental Section

Polystyrene-*block*-polyisoprene-*block*-polydimethyl-siloxane (coded as SID2)weer used in this study. In order to control the morphologies by using mixed solvent, we employed toluene and n-decane. TToluene is selective to PS and PI while n-decane is selective to PDMS. Four SID2 polymer solutions with different weight mixing ratio (1/2, 1/1.5, 1/1.3, 1/1.2) of toluene/ n-decane were prepared. The microdomain structures of SID2 triblock copolymers in the solution and in the bulk films cast from the corresponding solution were observed by SAXS.

Results and Discussion

The effects of different ratio between toluene and n-decane solvents on the microphase separation microdomain structures of SID2 triblock copolymer are demonstrated. Toluene prefers to stay in the PS phase while n-decane goes less into PS phase and more to the PI and PDMS phase. Figure 1 shows the mix solvent ratio dependence of SAXS profiles of different SID2 polymer solutions. The progressive addition of n-decane into toluene is found to induce a morphologi- cal transition, and various ordered microdomain structure is formed. Based on the SAXS result, at the mix weight ratio of 1/2 toluene/n-decane, the mi- cro-separated structure is spheres in BCC lattice. The hexagonally-packed cylinder is observed as the mix ratio is 1/1.5 toluene/n-decane. Lamellar structure can be obtained if the mix ration between toluene and n-decane is 1/1.3. For the toluene/ n-decane ration be- ing 1/1.2, which is the most similar to that of pure tol- uene used in casting process, shows the identical OTDD structure as observed in toluene-cast film. Furthermore, the hexagonally-packed cylinders and the lamellae are persisted in the bulk state cast from the corresponding solutions, indicating the morpholo- gies formed in the solution can be preserved down to cast bulk state. According to the results, mix-solvent can be used as a key technique for controlling and cre- ating a variety of ordered microdomain structures in SID triblock copolymers.

Table 1. Molecular Characteristics of SID2

Code	M_n ($\times 10^4$) (g・mol^{-1})	fPS	fPI	fPDMS	M_W/M_n
SID2	3.24	0.29	0.43	0.28	1.05

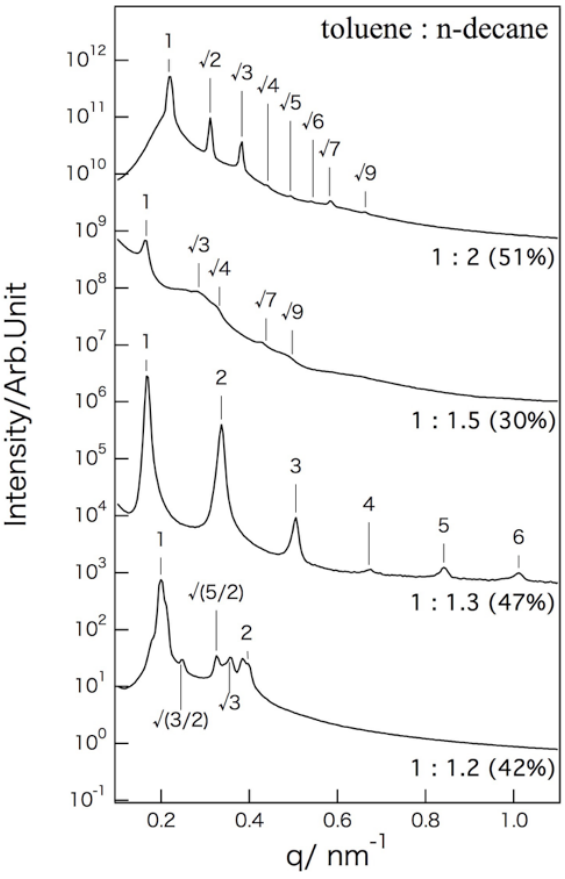

Figure 1 SAXS profiles of different ration between toluene/ n-decane for SID2 solution. The profiles are shifted vertically to avoid overlapping.

Oligomeric Structures of HSPB5 Variants

M. Yohda, K. Horiuchi, K. Hakamada, R. Inoue[1] and M. Sugiyama[1]

Department of Biotechnology and Life Science, Tokyo University of Agriculture and Technology

[1] *Institute for Integrated Radiation and Nuclear Science, Kyoto University*

INTRODUCTION: HSPB5 (also called αB-crystallin) is a member of small heat shock proteins that are characterized by a conserved α-crystallin domain (ACD) [1]. HSPB family members are known to form both homo -oligomeric and hetero-oligomeric complexes with other HSPBs. These complexes exhibit high rates of subunits exchange, suggesting to play a key role in substrate recognition and chaperoning functions. The HSPB5 mutation, R120G, is associated with both cataract and adult onset myopathy. When expressed in cells, the R120G mutant is associated with formation of amyloid-like oligomeric structures [2]. *In vitro*, recombinant R120G mutant protein forms soluble oligomers that are larger and more polydisperse than the wild type [3]. The mutation is partly rescued by the mutation of C-terminal IPI sequence, the conserved C-terminal 'IxI/V' motif, which is known to be responsible for the interaction between dimeric units. In this study, we examined the oligomeric structures of HSPB5 variants, the wild type (HSSPB5_WT), R120G mutant (HSPB5_R120G) and IPI mutant, in which IPI was replaced with AAA (HSPB5_IPI).

EXPERIMENTS: HSPB5 variants (HSSPB5_WT, HSPB5_R120G, HSPB5_IPI) were expressed in *E. coli* and purified by hydrophobic chromatography with Phenyl Sepharose and size-exclusion chromatography with Superdex 200. The molecular weights of the oligomers of HSPB5 variants were analyzed by Size-exclusion chromatography - multiangle light scattering (SEC–MALS) using a multiangle light-scattering detector (MINI DAWN, Wyatt Technology) and also Native- PAGE. The oligomeric conformation of HSPB5 variants were also analyzed by small angle X-ray scattering using NANO-PIX (RIGAKU)

RESULTS: By SEC-MALS, the molecular weights of the oligomers of HSPB5_WT and HSPB5_R120G determined to be 551kDa and 695kDa, respectively. The values are almost consistent with the results of Native PAGE. R120G appeared as a single band at the molecular weight of about 720 kDa. The wild type formed three bands with the molecular weights of approximately 480 kDa, 720 kDa and 960 kDa. Since the molecular mass of the monomer is about 20kDa, it is reasonable to think HSSPB5_WT forms the canonical 24meric complex of 480 kDa, which seems to have a nature to interact to form a large dimer (960kDa). On the contrary, HSPB5_R120G does not take 24meric conformation, but exists as stable 36mer (720 kDa). The wild type partly takes the same oligomeric conformation. Therefore, HSPB5_WT changes its oligomeric conformation between 24mer and 36mer, and HSPB5_R120G seems to lose the conformational change ability and stays at the 36meric conformation. The results of SAX analyses are shown in Fig. 1 and 2. The profiles of diffraction indicate that HSPB5_R120G is the largest and HSPB5_IPI is the smallest (Fig. 1). Fig. 2 shows the *Guinier* plots. The estimated R_g values of HSPB5 variants are as follow. R_g (HSPB5_WT) = 75.9 ± 3.6 A, R_g (HSPB5_R120G) =87.2 ± 4.3A, R_g (HSPB5_IPI) =85.9 ± 3.7A. Curiously, R_g of HSPB5_IPI is larger than that for HSPB5_WT.

We will further examine the oligomeric conformations of HSPB5 using various methods, SEC-MALS, SAXS, analytical ultracentrifuge and native mass spectrometry, and reveal the mechanism for the interaction with denatured proteins.

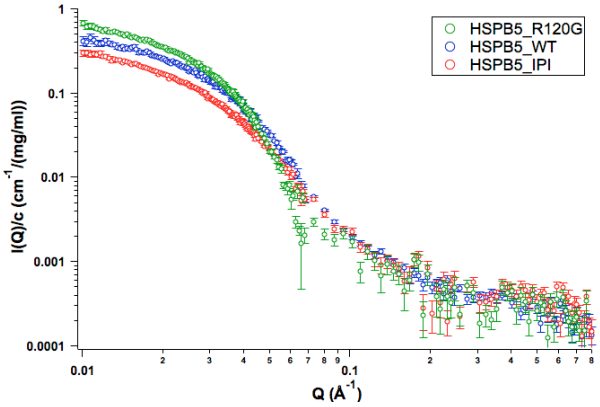

Fig. 1 SAXS profiles of HSPB5 variants

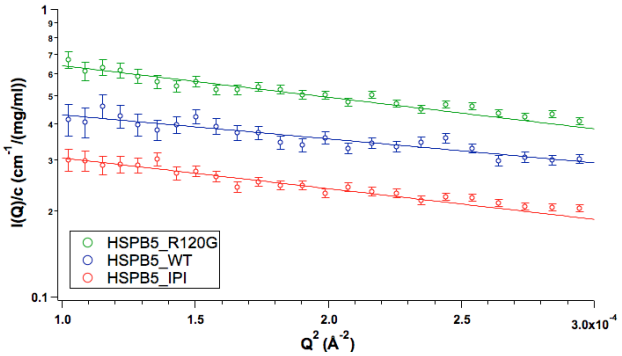

Fig. 2 *Guinier* plots of SAXS profiles

REFERENCES:

[1] E. Basha *et al.*, Trends. Biochem. Sci., **37** (2012) 106–117.

[2] A. Sanbe *et al.*, Proc. Natl. Acad. Sci. USA, **101** (2004) 10132–10136.

[3] M.P. Bova *et al.*, Proc. Natl. Acad. Sci. USA, **96** (1999) 6137–6142.

CO1-3 Effect of Cancer Associated Histone Mutations in the Nucleosome Structure

Y. Arimura, H. Kurumizaka and M. Sugiyama[1]
Faculty of Science and Engineering, Waseda University
[1]*Research Reactor Institute, Kyoto University*

INTRODUCTION: In chromatin, the nucleosome is the repeating unit, which is composed of two molecules of histones H2A, H2B, H3, and H4. These histones form a histone octamer, and about 150 base-pair DNA was wrapped around it [1]. Currently, mutations in the histone genes have been identified in cancer cells [2-4]. These histone mutations may directly disturb the chromatin structure and function.

Interestingly, in human cancer cells, mutations in canonical histone genes have been identified [2,5,6]. These finding are very surprising, because the human genome contains the multiple canonical histone genes. Therefore, This indicates that just one mutation of the multiple histone genes may have impact in cells. However, the mechanism by which the cancer-associated mutations of canonical histones impact on the chromatin structure and function has not been studied yet.

In several cancer cells, the H3.1 mutations in genes have been found [6]. Among these mutations, mutations with amino acid substitution at the H3.1 Glu97 residue are frequently found in cancer cells [7,8]. Therefore, we focused on the H3.1 Glu97 to Lys (H3.1 E97K) mutation. We then study how the H3.1E97K mutation affects the solution structure of the nucleosome. To do so, we performed small angle X-ray scattering (SAXS) experiments.

EXPERIMENTS: Human histones H2A, H2B, H3, and H4 were bacterially produced, and were purified near homogeneity. The 145 or 146 base-pair DNA was also produced in bacterial cells, and was purified. The histone octamer was first reconstituted with the purified histones H2A, H2B, H3, and H4, and was purified by gel filtration column chromatograghy. The purified histone octamer was then mixed with the 145 base pairs of DNA, and the nucleosome was reconstituted by the salt dialysis method. After the nucleosome was reconstituted, the nucleosome was further purified by a native polyacrylamide gel electrophoresis, using Prep Cell apparatus. The purified nucleosome fractions were collected, and the samples were concentrated by a filter cartridge, and the debris was removed by centrifugation. We then performed the SAXS experiments with the nucleosome. For the nucleosome containing histone mutations, we introduced the corresponding mutation in the histone genes. The histone mutants containing the animo acid substitutions were produced in bacterial cells, and were purified by the same method as the wild-type histone proteins. We then reconstituted the histone octamer with the mutant and wild type histones, and the nucleosomes were reconstituted by the salt dialysis method. The histone H2A-H2B dimer and H3-H4 tetramer may also be used as materials for the nucleosome reconstitution by the salt dialysis method, if the histone mutation may affect the histone octamer formation.

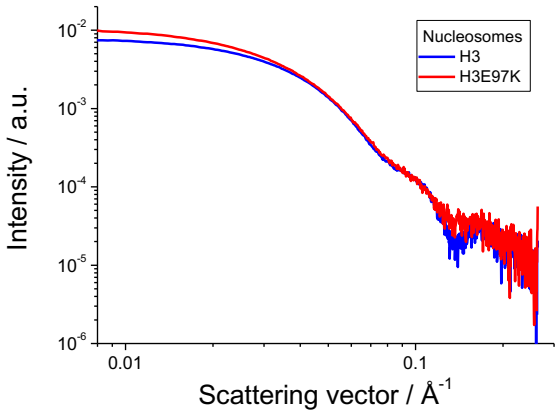

Fig. 1. SAXS profiles of the nucleosome containing H3E97K

RESULTS: As shown in Fig. 1, the SAXS curve was obtained with the nucleosome sample containing a histone mutation, and solution parameters of the nucleosome structure were estimated. A low resolution solution structure of the mutant nucleosome was obtained by Dummy atom modeling. The comparative study between solution structure and the X-ray structure of the mutant and wild type nucleosomes are underway.

REFERENCES:

[1] K. Luger *et al.*, Crystal structure of the nucleosome core particle at 2.8 A resolution. *Nature.*, **389** (1997) 251-260.
[2] J. Schwartzentruber *et al.*, Driver mutations in histone H3.3 and chromatin remodelling genes in paediatric glioblastoma. *Nature.*, **482** (2012) 226-231.
[3] G. Wu *et al.*, Somatic histone H3 alterations in pediatric diffuse intrinsic pontine gliomas and non-brainstem glioblastomas. *Nat Genet.*, **44** (2012) 251-253.
[4] S. Behjati *et al.*, Distinct H3F3A and H3F3B driver mutations define chondroblastoma and giant cell tumor of bone. *Nat Genet.*, **45** (2013) 1479-1482.
[5] C. Kandoth *et al.*, Mutational landscape and significance across 12 major cancer types. *Nature.*, **502** (2013) 333-339.
[6] I. Martincorena *et al.,* Somatic mutation in cancer and normal cells. *Science.*, **349** (2015) 1483-1489.
[7] E. Cerami *et al.*, The cBio cancer genomics portal: an open platform for exploring multidimensional cancer genomics data. *Cancer Discov.*, **2** (2012) 401-404.
[8] J. Gao *et al.*, Integrative analysis of complex cancer genomics and clinical profiles using the cBioPortal. *Sci Signal*, **6** (2013) 1.

CO1-4 **Nanostructure in Ferromagnetic Au Nanoparticles**

T. Sato, R. Sato, Y. Oba[1] and M. Sugiyama[2]

School of Integrated Design Engineering, Keio University

[1]*Materials sciences Research Center, Japan Atomic Energy Agency*

[2]*Institute for Integrated Radiation and Nuclear Science, Kyoto University*

INTRODUCTION: Nanoparticles often show physical properties different from bulk materials. Onset of ferromagnetism in the nanoparticles is one of the most attractive phenomena. In particular, it has been reported that Au nanoparticles with clean surface show ferromagnetism, while bulk Au is diamagnetic [1]. This ferromagnetism is free from surface modification by protective agents, which highly affect the magnetism of Au and sometimes obscure size effects [2,3]. However, the origin of the Au nanoparticles with no protective agents is still unclear. Although the magnetization and the coercivity vary among the samples, the size effects are not properly discussed because it is difficult to quantify the size in the strongly agglomerated nanoparticles.

Small-angle X-ray scattering (SAXS) is a powerful means to quantitatively characterize and compare the nanostructures among the samples. Therefore, the nanostructures in the ferromagnetic Au nanoparticles were characterized using SAXS in this study.

EXPERIMENTS: The samples were prepared by a gas evaporation method. SAXS measurements were performed using a SAXS instrument with Mo Kα radiation (Nano-viewer, RIGAKU) installed at the Institute for Integrated Radiation and Nuclear Science, Kyoto University. The characteristic X-ray emitted from Mo can penetrate heavy metals such as Au due to its high energy (17 keV). The sample-to-detector distance was 45 cm. During the SAXS measurements, the samples were put in vacuum to reduce the background scattering from air.

To measure low q region, an ultra-small-angle X-ray scattering (USAXS) instrument installed at the beam line BL19B2 in SPring-8 was also used [4]. Here, q is the magnitude of the scattering vector and is equal to $(4\pi/\lambda)\sin\theta$, where θ and λ are half the scattering angle and the wavelength of the incident X-ray. The energy of the incident X-ray was 18 keV. The obtained USAXS profiles were connected with the corresponding SAXS profiles. The analysis was carried out using the connected profiles.

RESULTS: Fig. 1 shows a typical scattering profile of the Au nanoparticles. The profile has a shoulder around q=0.1 nm^{-1}. This indicates that the nanostructure is formed in the sample. The average diameter of the nanostructure is estimated to 51 nm using curve fitting analysis with the assumption that the nanoparticles are spherical. In the previous study [1], the Au nanoparticles with the average diameter of a few nm were observed using a transmission electron microscope (TEM). Therefore, the nanostructure observed using the SAXS and USAXS is the agglomerates of the Au nanoparticles. The clean surface of the Au nanoparticles probably induces the agglomeration of the Au nanoparticles.

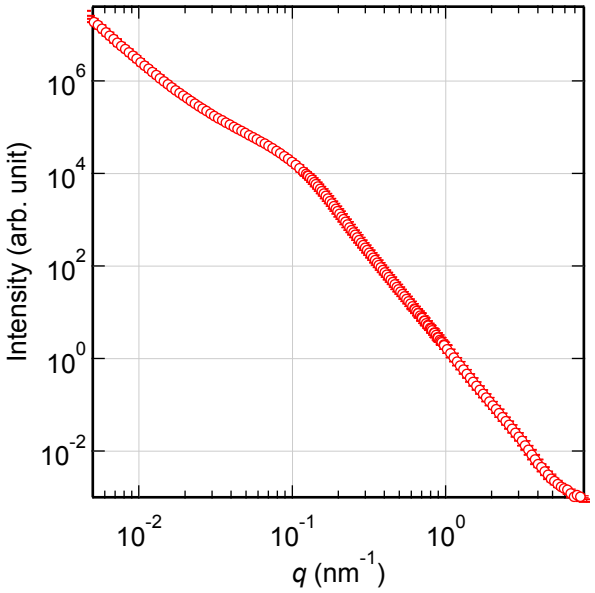

Fig. 1. Typical scattering profile of the Au nanoparticles with clean surface. The profile is composed of the USAXS (q<1 nm^{-1}) and SAXS (q>0.6 nm^{-1}) profiles. The intermediate region (0.6<q<1 nm^{-1}) was measured using both USAXS and SAXS.

The previous study reported the coercivity over 10 Oe even at room temperature. This is unrealistic value for the nanoparticles with the diameter of a few nm. Therefore, the formation of the agglomerates is probably related with this coercivity.

REFERENCES:

[1] R. Sato *et al.*, J. Magn. Magn. Mater., **393** (2015) 209-212.

[2] P. Crespo *et al.*, Phys. Rev. Lett., **93** (2004) 087204/1-4.

[3] Y. Yamamoto *et al.*, Phys. Rev. Lett., **93** (2004) 116801/1-4.

[4] K. Osaka *et al.*, AIP Conf. Proc., **1741** (2016) 030003/1-4.

Development of Neutron Imager Basded on Hole-type MPGD with Glass Capillary Plate

F. Tokanai[1], R. Itoh[2], S. Ishizawa[2], T. Moriya[1], M. Takeyama[1], T. Sumiyoshi[3], H. Kondo[4], H. Sugiyama[4], M. Hayashi[4], T. Okada[4], M. Hino[5]

[1]*Department of Physics, Yamagata University*
[2]*Graduate School of Science and Engineering, Yamagata University*
[3]*Graduate School of Science and Engineering, Tokyo Metropolitan University*
[4]*Electron Tube Division, Hamamatsu Photonics K.K.*
[5]*Research Reactor Institute, Kyoto University*

INTRODUCTION: Neutron imaging is more useful than X-ray imaging for light elements in the sample such as hydrogen, lithium, boron, carbon, and nitrogen. Owing to their unique ability to probe inside samples, neutrons have been widely utilized for neutron radiography in various fields, including fundamental science, archaeology, and industry. A new beam line has recently been constructed at Japan proton accelerator research complex (J-PARC) for pulsed neutron imaging [1], and several compact accelerator-driven neutron sources are now available for non-destructive testing [2] or for boron neutron capture therapy (BNCT). High-resolution imaging capability with a moderate effective area is required in practical applications of neutron sources. We have been developed an optical imaging capillary plate (CP) gas detector for high-resolution neutron imaging [3]. The performance of the neutron imager was investigated using a cold neutron beam line CN-3 in Kyoto University Reactor (KUR)

EXPERIMENTS: Fig. 1 shows the experimental setup of the neutron gas scintillation imager (n-GSI). It consists of a thin layer of ^{10}B to convert neutron, a CP gas detector filled with a Ne-based gas mixture at 1 atm, mirror and lens optics, and a cooled CMOS camera system. CP has an effective diameter 25 mm and a thickness, individual hole diameter, and pitch of 300 μm, 50 μm, and 64 μm, respectively. The neutron wavelength of maximum intensity and total flux of the CN-3 guide tube were 2 Å and 3.8×10^6 neutron cm^{-2} s^{-1}, respectively. The n-GSI system was placed 250 mm away from the downstream exit of the neutron guide. The neutrons were irradiated through a test chart made by using a Gd slit on a thin glass sheet.

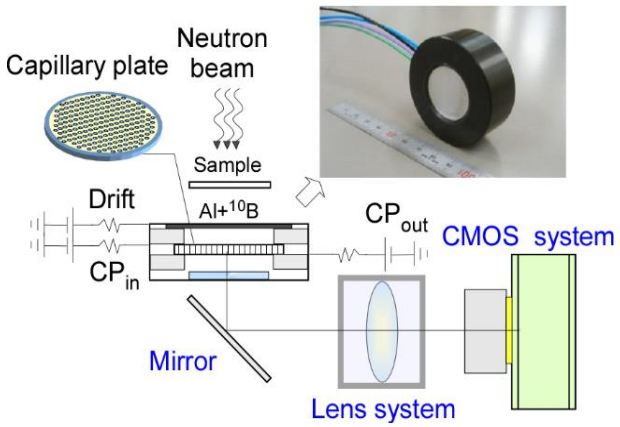

Fig. 1 Schematic view of n-GSI and experimental arrangement for the performance of neutron beams from KUR.

RESULTS: Fig. 2 shows the neutron transmission image of the test chart obtained by n-GSI system. The exposure time was 300 s. The numerical number in Fig.2 indicates the width of the slit on the chart. The practical position resolution of n-GSI is estimated to be 200 μm for the neutron beam. To improve the position resolution, we have been currently developing a new n-GSI system.

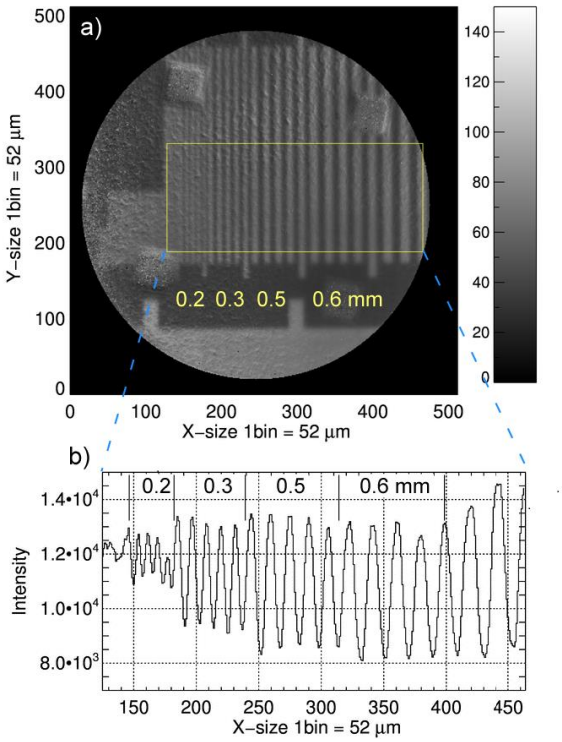

Fig. 2. a) Neutron image of a neutron test chart obtained by n-GSI system. The CP gas detector was filled with Ne (90%) + CF_4 (10%) at 1atm. b) the intensity projection on the x-axis for the yellow rectangular box in the neutron image.

REFERENCES:

[1] T. Shinohara *et al.*, J. Phys.: Conf. Ser. **746** (2016) 012007K.
[2] Y. Ikeda *et al.*, Nucl. Instr. and Meth., **833** (2016) 61-67.
[3] T. Sumiyoshi *et al.*, Hamon **27** (1) (2017) 16-19.

CO1-6 Current Status of B–3 Beam Port of KUR, 2017

K. Mori, R. Okumura, H. Yoshino, S. Sato[1], H. Hiraka[2], K. Iwase[3], and A. Okumura[4]

Institute for Integrated Radiation and Nuclear Science, Kyoto University (KURNS)
[1]High Energy Accelerator Research Organization (KEK)
[2]Neutron Science Center, Korea Atomic Energy Research Institute
[3]Department of Materials and Engineering, Ibaraki University
[4]Graduate School of Engineering, Kyoto University

INTRODUCTION: Neutron diffraction is a powerful tool to determine precisely the positions of light elements (e.g., hydrogen and lithium) in solids. This is the main reason why neutron powder diffractometers are critical for structural investigations of energy storage materials, for example, rechargeable lithium-ion batteries and hydrogen absorbing alloys. The B–3 beam port of Kyoto University Research Reactor (KUR) had long been used as a four-circle single-crystal neutron diffractometer (4CND). For the last decade, however, the 4CND was so old that its research activity on neutron science was quite low. Now, the compact multipurpose neutron diffractometer (CMND) is installed on the B-3 beam port of KUR.

SPECIFICATIONS: Fig. 1 shows the current state of the CMND. The CMND is equipped with a new beam shutter manufactured by the KURNS factory. In addition, the CMND has a wide space around the sample; therefore, we can easily install any other system. The neutron wavelength, λ, which is monochromatized by the (220) plane of a Cu single crystal (i.e., Cu monochromator), is 1 Å. To cover the detector area of $6\,° \leq 2\theta \leq 150\,°$, twenty-five ^{3}He tube detectors (1/2 inch in diameter) are used (see Fig. 2), where 2θ is the scattering angle. A detector bank including the twenty-five ^{3}He tube detectors is placed on an arm of the HUBER-440 goniometer. The distance from the Cu monochromator to the sample is approximately 2 m, and the distance from the sample to the detector is 1.2 m.

PRELIMINARY EXPERIMENTS: The preliminary neutron diffraction experiments were performed using a nickel (Ni) powder sample. Figs. 3(a) and (b) show the neutron powder diffraction data of Ni collected on the B-3 beam port and the X-ray powder diffraction data of Ni collected on the Laboratory X-ray diffractometer with a Cu$K\alpha$ radiation, respectively. As shown in Fig. 3(a), we succeeded to observe several Bragg reflections of Ni. In particular, the Bragg reflections at the high Q region (corresponding to the high 2θ region) could be observed using the CMND, where Q is the magnitude of the scattering vector ($= 4\pi\sin\theta/\lambda$, where θ is half of the scattering angle, 2θ). The complementary use of neutron and X-ray diffraction is very useful for the structural investigations. Further improvements are now in progress.

Fig. 1. The compact multipurpose neutron diffractometer, installed at the B-3 beam port of KUR.


Fig. 2. Twenty-five ^{3}He tube detectors (1/2 inch in diameter) on the detector bank.

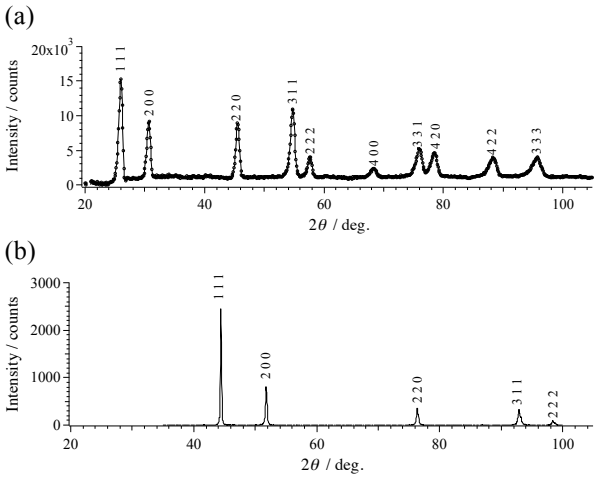

Fig. 3. Diffraction data of the nickel (Ni) powder: (a) neutron (B-3 beam port) and (b) X-ray (Cu$K\alpha$ radiation), respectively.

CO1-7 Study of the Properties of Water and the Physiological Activation Phenomena by using High-Intensity Pulsed Coherent Radiation

S. Okuda, Y. Tanaka and T. Takahashi[1]

Graduate School of Engineering, Osaka Prefecture University
[1]Research Reactor Institute, Kyoto University

INTRODUCTION: The coherent transition radiation (CTR) from electron bunches of a linear accelerator (linac) has continuous spectra in a submillimeter to millimeter wavelength range corresponding to the terahertz (THz) frequency range. It is a picosecond pulsed light and hence, has extremely high peak-intensities compared with the other THz light sources. The light source system using the CTR from the electron beams of the 45 MeV L-band electron linac was established at Kyoto University Research Reactor Institute (KURRI) [1-3]. This CTR light source developed has been applied to absorption spectroscopy. Recently, the possibility of any nonlinear effects was found in the measurement of the absorption spectroscopy at KURRI.

The important application of the light source is the investigation of the biological effects of the CTR. The main purpose of the present work is the investigation of the biological effects of the high-intensity pulsed CTR.

EXPERIMENTAL METHOD: The electron linac at KURRI was used in the experiments. In most experiments the beam energy, macropulse length and the repetition rate are 42 MeV, 47 ns and 60 Hz, respectively. The experimental configurations for the absorption spectroscopy are schematically shown in Fig. 1. The output CTR light from a light source chamber was transported out from the accelerator room. The spectrum of the light after passing through the sample was measured with a Martin-Puplett type interferometer and a liquid-He-cooled silicon bolometer. The wavenumber resolution was 0.1 cm^{-1}. The incident light was divided to two parts with the same light intensity in the interferometer. In this system the absorption spectroscopy and the irradiation were carried out at the same time.

In the absorption spectroscopy the sample was located on the light path between the interferometer and the detector. The thickness of the liquid sample was about 100 μm, which was sandwiched with two anhydrous quartz plates 3 mm thick. The light was focused at a light collimator 8 mmϕ in diameter located before the sample. The details of the methods for the measurements are described in ref. 2 and 3. The liquid samples used in the experiments were water, aqueous solutions of NaCl for the investigation of the basic behaviors of the absorbed light in the analysis of the biological effects by the irradiation of CTR.

In the irradiation experiments of the CTR several kinds of bacillus, human culture cell and microorganism were used. After the irradiation the physiological activation phenomena were investigated. The new system for observing the sample during the CTR irradiation experiments is under preparation.

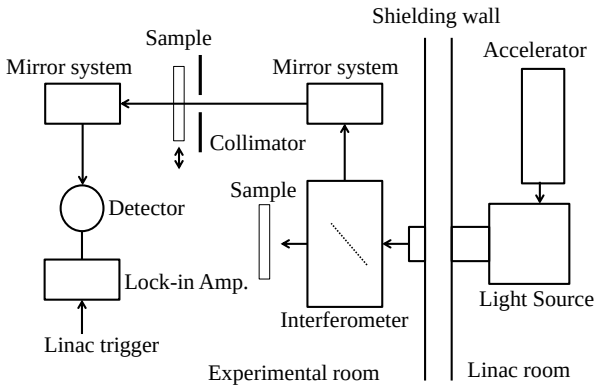

Fig. 1. Schematic diagram showing the configurations for absorption spectroscopy and irradiation experiments using the CTR

RESULTS AND DISCUSSION: The characteristics of the CTR light source were investigated, and the electron beam conditions and the experimental configurations were optimized. The light spectrum was sufficiently stable during the measurements within ±2-3% in a wavenumber range of 4-13 cm^{-1}. The spectrum had a peak at a wavenumber of about 7 cm^{-1}. If a band-pass light filter or a grating-type monochromator is used in order to avoid the influence of the main part of the spectrum around the peak the wavenumber range would be expanded to 2-35 cm^{-1}, which is determined by the specification of the detector. The intensity of light was estimated to be about 10^{-7} W/0.1%b.w. and was found to be sufficiently high even if it becomes 10^{-6} of the initial one after transmission through the sample due to absorption. The micropulse length of the CTR which corresponds to that of the electron beam from the linac was evaluated by the interferogram to be about 3 ps. Such a relatively short pulse length is due to the special bunching process in the optimized operational conditions of the linac. These results indicate that the peak light intensity in the micropulse is about 10^4 W. While the averaged CTR power is sufficiently low to induce thermal effects, the comparatively high peak power might cause any nonlinear effects.

In the irradiation experiments of CTR to investigate the biological effects the experimental conditions have been optimized. Preliminary results have been obtained by the CTR irradiation so far. 4 hours irradiation of CTR did not cause any effects on human fibroblast cells as the estimations of rate of living cells and rate of DNA segmentation.

REFERENCES:

[1] T. Takahashi *et al.*, Rev. Sci. Instrum. **69** (1998) 3770.
[2] S. Okuda and T. Takahashi, Infrared Phys. Technol. **51** (2008) 410.
[3] S. Okuda and T. Takahashi, J. Jpn. Soc. Infrared Science & Technology 25 (2016) 49 (in Japanese).

First Neutron Focusing Test with a Couple of 900mm Long Ellipsoidal Supermirrors

M. Hino, T. Hosobata[1], T. Oda, H. Yoshinaga, S. Takeda[1], Y. Yamagata[1], H. Endo[2], N.L. Yamada[2] and Y. Kawabata

Institute for Integrated Radiation and Nuclear Science, Kyoto University (KURNS), Japan
[1]RAP, RIKEN, Japan
[2]IMSS, KEK, Japan

INTRODUCTION: Progress of neutron optical devices is very significant. Recently we proposed promising fabrication method for aspherical focusing supermirror with metal substrate [1-4]. The metallic substrate is robust and ductile, to which able to fabricate steeply curved surface with high form accuracy. It is also applicable to use under high radiation irradiation and high-temperature filed, even at a place close to the neutron target and moderator. Furthermore, it is possible to fabricate a large focusing mirror by combining multiple segmented mirrors with mechanical fastening entailing the usage of screw holes and fixture tabs. The big problem was required surface roughness for neutron mirror. The roughness should be smaller than 0.3 nm for high-*m* supermirror coating. Here *m* is the maximum critical angle of the mirror in units of critical angle of natural nickel. By using electroless nickel-phosphorus (Ni-P) plating, we overcame the problem and are establishing fabrication process for aspherical focusing supermirror. In this study, we show a latest result for neutron focusing experiment with a couple of ellipsoidal supermirrors with metallic substrates.

EXPERIMENTS: We fabricated ellipsoidal metallic substrates with the Ni-P plating, based on the technology using ultrahigh precision cutting with correction processing, followed by mechanical precision polishing. The first precise manufacturing was conducted at a CNC machine for development of neutron optical devices at workshop of KURNS. The ultra-precise manufacturing, polishing and cleaning of the metallic substrate were conducted at RIKEN. The supermirror coating was conducted with KUR-IBS [5]. The neutron experiments were conducted at CN-3 beam line at KURNS and the BL06 (VIN ROSE) beam port at J-PARC MLF [6].

RESULTS: We fabricated a couple of *m*=3 NiC/Ti ellipsoidal supermirrors in which length of 900mm. The semi-major and semi-minor axes of the ellipsoidal supermirror were 1250 mm and 65.4 mm, respectively. The acceptable angle of the minor axis arc of the ellipsoidal supermirror is 20 degree. The two ellipsoidal supermirrors were placed between Φ1mm pinhole and a two-dimensional position sensitive neutron detector as shown in Fig.1. The distances between the pinhole and the detector was 5 m and that between the two ellipsoidal supermirrors was 2.5m. Here Φ10mm pinhole was placed 100 mm before the detector to reduce background neutrons. With the ellipsoidal mirrors, as shown in Fig 1(b), the intensity image was circular spot and the spot size was almost equivalent to that of the Φ1mm pinhole. Without the mirrors, the intensity image was not clear peak. Figure 1(c) shows TOF spectra with and without mirrors. Here the intensity without mirror was multiplied by 100 and that of wavelength 1nm or more was very little. On the other hand, the wavelength of peak intensity was longer than 1 nm because the available wavelength of neutrons reflected by the *m*=3 ellipsoidal supermirrors is longer than 1nm. It is possible to expand the available wavelength with higher-*m* supermirrors. In this study, it is clearly demonstrated that dramatically intensity gain for long wavelength neutrons reflected by the two *m*=3 ellipsoidal supermirrors.

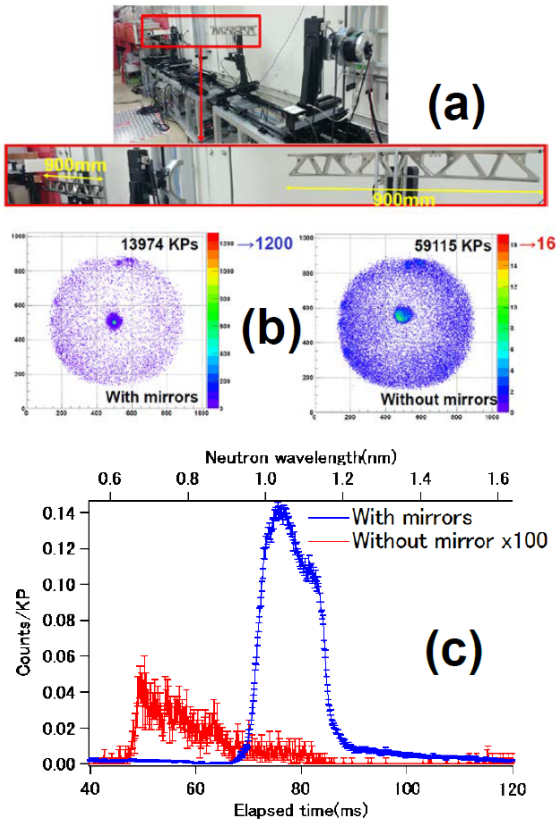

Fig. 1. (a) Photograph of the experimental setup for double ellipsoid neutron supermirrors at the BL06 at the J-PARC MLF. (b) Neutron intensity image at focal position with and without the ellipsoidal neutron supermirrors. (c) TOF spectra of neutrons reflected with and without the ellipsoidal neutron supermirrors. The intensity without mirror was multiplied by 100.

REFERENCES:

[1]J.Guo, *et al.*, Optics Express 22(2014) 063108.
[2]J.Guo, *et al.*, Review of Scientific Instruments 86(2015) 86(2015) 063108.
[3] S.Takeda, *et al.*, Optics Express 24(2016) 12478.
[4] T.Hosobata, *et al.*, Optics Express 25(2017) 20012.
[5] M.Hino, *et al.*, Nucl. Instr. and Meth., **797**(2015) 265.
[6] M.Hino, *et al.*, J. Nucl. Sci. Technol. 54(2017), 1223.

CO1-9 Hydrogen Retention on Plasma Facing Material Irradiated by High Energy Particle Beam

K. Tokunaga, M. Matsuyama[1], K. Araki, M. Hasegawa, K. Nakamura and Q. Xu[2]

Research Institute for Applied Mechanics, Kyushu University
[1]Hydrogen Isotope Research Center, University of Toyama
[2]Research Reactor Institute, Kyoto University

INTRODUCTION: It is of importance to clarify phenomena of implantation, retention, diffusion and permeation of tritium on surface of the armor materials of the first wall/blanket and the divertor on fusion device from a viewpoint of precise control of fuel particles, reduction of tritium inventory and safe waste management of materials contaminated with tritium (T). Refractory metals such as tungsten (W) is potential candidate for an armor of the first wall and the divertor plate of the fusion reactor because of its low erosion yield and good thermal properties. The armor material will be subjected to heavy thermal loads in the steady state or transient mode combined with high energy neutron irradiation that will cause serious material degradation. In addition, high energy runaway electrons would bombard the armor materials along the equatorial plane in fusion device. It is considered that these cause radiation damage and enhance tritium retention. In the present works, T exposure experiments have been carried out on W samples which were irradiated by high energy electrons using LINAC in KURRI of Research Reactor Institute, Kyoto University to investigate effects of high energy electrons irradiation and microstructure on tritium retention of W. In this fiscal year, pure W and recrystallized W were irradiated by high energy electron beam. After that, positron annihilation experiment was carried out to identify the radiation defect. In addition, tritium exposure experiments have been carried out using a tritium (T) exposure device.

EXPERIMENTS: W samples used were ITER grade W (IG-W) and recrystallized W. In the case of IG-W, one was W sample (ITER grade W(1)) which the surface were manufactured to be oriented parallel to the rolling surface and rolling direction. The other W sample (ITER grade W(3)) which the surface were manufactured to be oriented perpendicular to the rolling surface and rolling direction. On the other hand, heat treatment was performed at 1800 °C for 1h at high vacuum to recrystallize IG-W. The sizes of W samples were 10mm x 10mm x 1mm. The surface of the both samples were polished to be mirrored. High energy electrons irradiation has been carried out using LINAC in KURRI of Research Reactor Institute, Kyoto University. An energy of electron irradiated was 10 MeV and DPA was 2.8 x 10^{-3}. Temperature during the irradiation was measured by thermocouples which was contacted with a backside of the W samples. After the electron beam irradiation, positron annihilation experiment was carried out. In addition, T exposure experiments have been carried out using a T exposure device in University of Toyama. Pressure of the T gas was 1.3 kPa and T exposure was kept for 4 h. T concentration in the gas was about 5 %. Temperatures of pre-heating and T exposures were 100 °C. After the exposure to T gas, T amount retained in surface layers of the sample was evaluated by β-ray-induced X-ray spectrometry (BIXS) and imaging plate (IP) measurements.

RESULTS: Figure 1 shows amount of T measured by the IP measurement. In the case of non-irradiated samples, T retention of non-recrystallized samples is larger than that of recrystallized samples. These results indicated that some kinds of defects which can trap T decreased by the recrystallization. After the electron beam irradiation, amount of T of samples increases. In particular, in the ca of the recrystallized samples, the amounts of T of electron beam irradiated samples are a few times of that of non-irradiated samples. Positron annihilation experiment indicated that the electron irradiation made life time of τ_2 small and intensity of I_2 increased. This result means that small defects were induced and concentration of the defects increased in the recrystallized sample by the electron irradiation. As a result, it is considered that these kinds of defects trap T. Quantitative evaluation is currently underway.

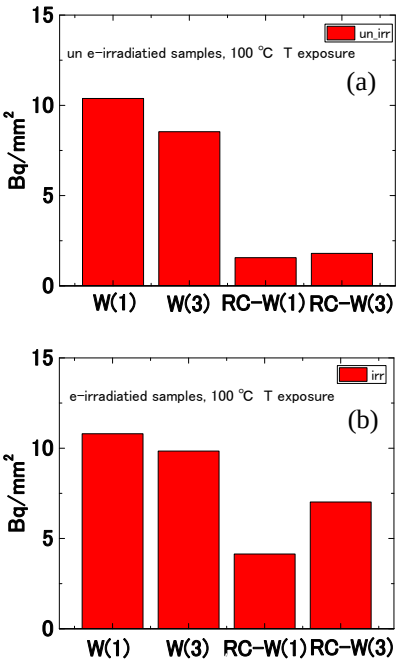

Fig. 1. Amount of tritium on before(a) and after(b) electron beam irradiation measured by IP measurement. RC-W(1) and RC-W(3) are recrystallized W(1) and W(3), respectively.